TISSUE ENGINEERING: Part C
Volume 24, Number 5, 2018

DOI: 10.1089/ten.tec.2017.0531

termis
Tissue Engineering
& Regenerative Medicine
International Society

METHODS ARTICLE

Freezing Responses in DMSO-Based Cryopreservation of Human iPS Cells: Aggregates Versus Single Cells

Rui Li, BS,[1,*] Guanglin Yu, PhD,[2,*] Samira M. Azarin, PhD,[3] and Allison Hubel, PhD[2]

Inadequate preservation methods of human induced pluripotent stem cells (hiPSCs) have impeded efficient reestablishment of cell culture after the freeze–thaw process. In this study, we examined roles of the cooling rate, seeding temperature, and difference between cell aggregates (3–50 cells) and single cells in controlled rate freezing of hiPSCs. Intracellular ice formation (IIF), post-thaw membrane integrity, cell attachment, apoptosis, and cytoskeleton organization were evaluated to understand the different freezing responses between hiPSC single cells and aggregates, among cooling rates of 1, 3, and 10°C/min, and between seeding temperatures of −4°C and −8°C. Raman spectroscopy images of ice showed that a lower seeding temperature (−8°C) did not affect IIF in single cells, but significantly increased IIF in aggregates, suggesting higher sensitivity of aggregates to supercooling. In the absence of IIF, Raman images showed greater variation of dimethyl sulfoxide concentration across aggregates than single cells, suggesting cryoprotectant transport limitations in aggregates. The ability of cryopreserved aggregates to attach to culture substrates did not correlate with membrane integrity for the wide range of freezing parameters, indicating inadequacy of using only membrane integrity-based optimization metrics. Lower cooling rates (1 and 3°C/min) combined with higher seeding temperature (–4°C) were better at preventing IIF and preserving cell function than a higher cooling rate (10°C/min) or lower seeding temperature (–8°C), proving the seeding temperature range of −7°C to −12°C from literature to be suboptimal. Unique f-actin cytoskeletal organization into a honeycomb-like pattern was observed in post-passage and post-thaw colonies and correlated with successful reestablishment of cell culture.

Keywords: cryopreservation, induced pluripotent stem cells, dimethyl sulfoxide, Raman spectroscopy

Introduction

Human induced pluripotent stem cells (hiPSCs) are multicellular aggregates that can be reprogrammed from a variety of somatic cells and have the potential to be differentiated into all three germ layers,[1,2] attracting much interest in tissue engineering,[3–5] disease modeling,[6,7] and personalized medicine.[8,9] For both clinical and scientific purposes, effective cryopreservation of hiPSCs is required for transportation, storage of frozen hiPSCs, and other downstream uses. However, cryopreserved hiPSCs are vulnerable to loss of viability, function, or pluripotency.[10–12] hiPSCs can be frozen either as aggregates or single cells depending upon the application.

Cryopreservation of hiPSCs typically involves two different methods: conventional slow cooling and vitrification. Briefly, vitrification uses high concentrations of cryoprotective agents combined with high cooling rates to avoid the formation of ice during freezing. Conventional slow cooling in this particular application implies using a solution using 10% dimethyl sulfoxide (DMSO) and a cooling rate of 1°C/min. High rates of post-thaw recovery are observed ($\sim$100%) by vitrification, but the method faces limitations of poor scalability and high risk for contamination.[13] Slow-cooling studies have attempted to find suitable freezing parameters for cells.[14–18]

ROCK inhibitor (ROCKi) Y-27632 has been used to enhance the survival of dissociated hiPSCs (i.e., single cells).[19–21] Disruption of nonmuscle myosin IIA (NMMIIA) and actin as a result of ROCK inhibition has been shown to increase survival and pluripotency of single hiPSCs.[22,23] However, the addition of ROCKi can have contradictory effects in the case of hiPSC aggregates. The downregulation of NMMIIA has been shown

Departments of [1]Biomedical Engineering, [2]Mechanical Engineering, and [3]Chemical Engineering and Materials Science, University of Minnesota, Minneapolis, Minnesota.
*These two authors contributed equally to the work.

to impair cell adhesion, cell–cell junctions, self-renewal, and pluripotency of hiPSC aggregates.[24,25] To exclude the confounding effect of ROCKi and capture native cell response to freezing, we hereby studied the cryopreservation of hiPSCs without the use of ROCKi.

Despite attempts to improve cryopreservation of multicellular aggregates, the mechanisms of damage for different freezing conditions are poorly understood. As with single cells, extensive intracellular ice formation (IIF) has been proven to be damaging[26]; exposure to high solute concentration at low temperatures can cause the solute effect in cells, and the addition or removal of cryoprotectants can result in osmotic stress.[11] However, freezing responses of cell aggregates are more complex than single cells. For example, propagation of IIF in cell aggregates through gap junctions has been observed experimentally in a variety of cell types.[27–29]

Recently, Raman spectroscopy has become a powerful tool for understanding cell responses to the freezing environment.[30–34] The magnitude and spatial distribution of specific chemical signals (liquid water, ice, cryoprotectant, hydrohalite) and biological signals (cytochrome c) have been measured for single cells during freezing.[34,35] However, to the best of our knowledge, there has been no Raman spectroscopy study of cell aggregates. In this study, Raman spectroscopy was used to observe both hiPSC single cells and aggregates frozen at three cooling rates and two seeding temperatures. The seeding temperature is the temperature at which ice forms in the extracellular solution (Fig. 1A).

In parallel, hiPSCs as single cells or aggregates were frozen using a programmable controlled rate freezer (CRF) with the same cooling rates and seeding temperatures as Raman spectroscopy. Cell recovery, attachment, apoptosis, and cytoskeletal organization were examined after rapid thawing in a 37°C water bath. This work will deepen our understanding of behaviors of single cells and aggregates frozen at various conditions and promote the development of improved cryopreservation protocols for hiPSCs.

Materials and Methods

Cell culture and phenotyping

The hiPSC line DF-19-9-11 was reprogrammed by Yu & Thomson.[2] hiPSCs were cultured on Matrigel (hESC-qualified, LDEV-free; Corning) in essential 8 medium (Thermo Fisher) in a 37°C incubator at 5% CO_2. Cells were passaged as aggregates using the enzyme-free dissociation

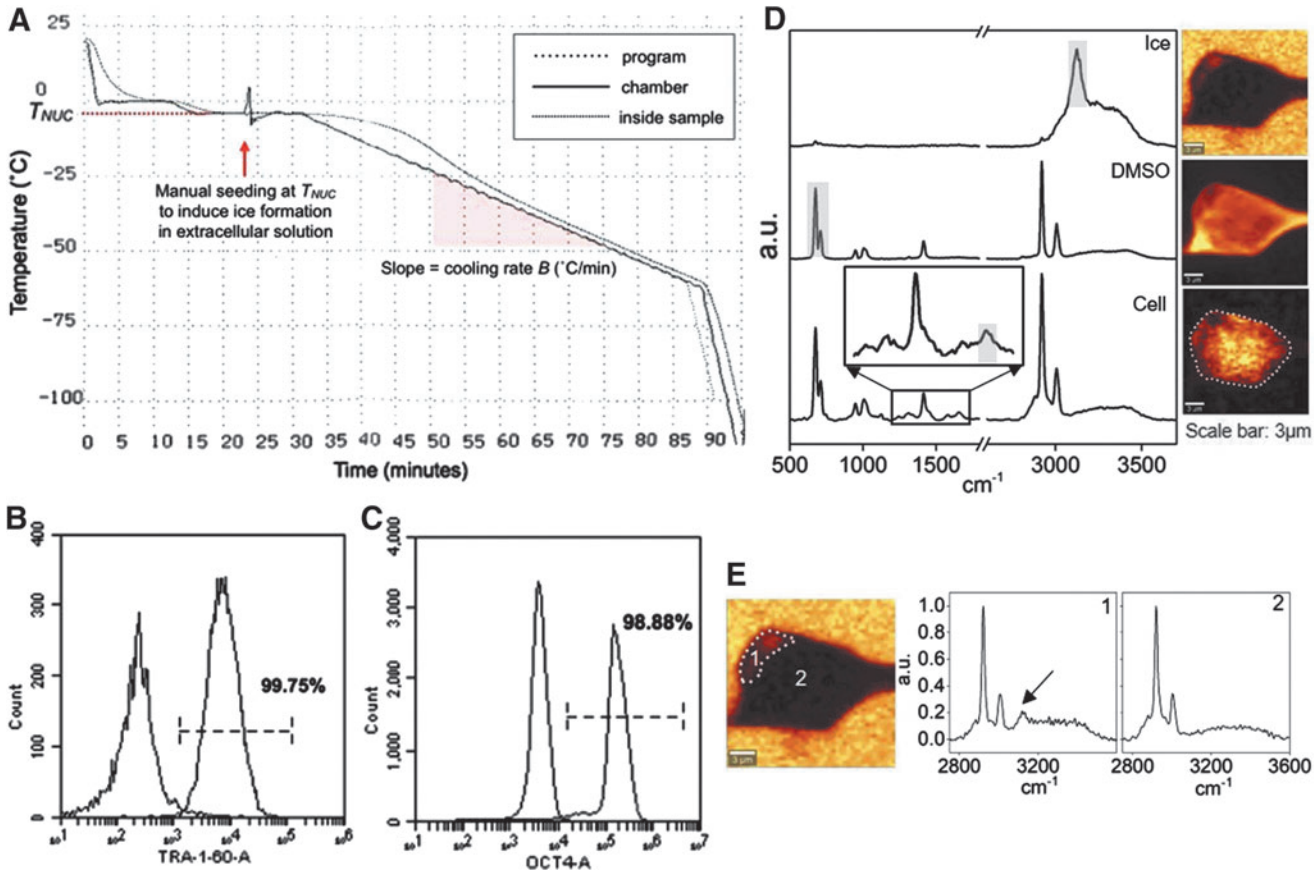

FIG. 1. **(A)** A CRF cooling curve showing a cooling rate of 1°C/min and seeding temperature of –4°C. **(B)** Flow cytometry overlaid histograms of anti-TRA-1-60 and its isotype control, showing 99.75% TRA-1-60-positive cells. **(C)** Flow cytometry overlaid histograms of anti-OCT4 and its isotype control, showing 98.88% OCT4-positive cells. **(D)** Raman spectra of ice (in arbitrary units, a.u.), DMSO, and single hiPSCs cryopreserved in 10% DMSO. Raman images of ice, DMSO, and amide I are rendered based on the specific Raman signal indicated on the spectra. **(E)** Raman image of ice showing cell section with IIF (1) and without IIF (2) with corresponding Raman spectra. The *arrow* indicates Raman signal of ice. CRF, controlled rate freezer; DMSO, dimethyl sulfoxide; hiPSCs, human induced pluripotent stem cells; IIF, intracellular ice formation.

reagent ReLeSR (STEMCELL Technologies). hiPSC cultures were routinely tested for mycoplasma using the MycoAlert PLUS detection kit (Lonza). Cells were >95% positive (Fig. 1B, C) for hiPSC pluripotency surface marker TRA-1-60 (BD Biosciences) and transcription factor OCT4 (BioLegend), determined using flow cytometry.

Cell dissociation

Freezing studies were performed using single cells or small aggregates (3–50 cells). Aggregate size was controlled by the amount of gentle pipetting. Aggregates were dissociated into single cells using accutase (Innovative Cell Technologies).

Controlled rate freezing

Aggregates and single cells resuspended in 10% DMSO in 1 × phosphate-buffered saline containing Ca^{2+} and Mg^{2+} were transferred into cryovials and incubated at room temperature for 30 min before freezing. Cryovials were frozen using a CRF (Planer Series III Kryo 10) following the steps listed below with a cooling rate, B, of 1, 3, or 10°C/min and a seeding temperature, T_{NUC}, of −4°C or −8°C:

1. Starting temperature 20°C
2. −10°C/min to 0°C
3. Hold at 0°C for 10 min
4. B°C/min to T_{NUC}°C
5. Hold at T_{NUC}°C for 15 min; induce ice nucleation by manual seeding when sample temperature stabilizes at T_{NUC}°C
6. B°C/min to −60°C
7. −10°C/min to −100°C

Manual seeding was achieved by spraying liquid nitrogen briefly onto the outer surface of a cryovial using CRYOGUN (Brymill). Frozen cryovials were thawed in a 37°C water bath. Cryovials were submerged partially below the lid and agitated for ∼2 min. Cells were assessed immediately post-thaw.

Post-thaw viability and function

Cells were singularized using Accumax (Innovative Cell Technologies) and stained for viability by membrane integrity using acridine orange and propidium iodide. Counts were obtained both prefreeze and post-thaw for all samples. The post-thaw recovery rate was calculated as the percentage of post-thaw live cell count divided by prefreeze live cell count.

Post-thaw function was assessed by quantifying the attachment rate of thawed cells. Passaged fresh cells served as controls. Seeding density was kept constant based on the post-thaw live cell count. Cells were cultured on Matrigel, undisturbed for 24 h, and stained for viability using calcein AM and propidium iodide. The stained cells were read to obtain fluorescence levels using a microplate reader (BioTek Synergy HT) with ex/em 485/528 nm and 530/590 nm filter sets. The post-thaw attachment rate was calculated as the ratio of the calcein AM fluorescence level of each thawed sample to the mean calcein AM fluorescence level of passaged controls.

Post-thaw apoptotic subpopulations

Early and late apoptosis subpopulations were determined using flow cytometry post-thaw for cell aggregates. Cells were singularized with Accumax and stained for polycaspase activation using FLICA FAM-VAD-FMK antibody (Immunochemistry Technologies) and for loss of membrane integrity using 7-AAD (BD Via-Probe; BD Biosciences). Apoptosis was induced using camptothecin (Adipogen) and cell death was induced by incubating cells at 60°C for 15 min and 4°C for 5 min to serve as gating controls. Early apoptotic cells were defined as positive for FLICA and negative for 7-AAD staining, late apoptotic cells as positive for both FLICA and 7-AAD, necrotic cells as negative for FLICA and positive for 7-AAD, and live cells as negative for both FLICA and 7-AAD.

Post-thaw time course assessments

Cells that successfully attached 24 h post-thaw were fixed and stained to detect chromatin condensation using Hoechst 33342 (Thermo Fisher) and f-actin organization using rhodamine phalloidin (Thermo Fisher) at 4, 8, 12, and 24 h post-thaw. Fresh cells were fixed and stained for nucleic acid and f-actin at 4, 8, 12, and 24 h postpassage to be compared with post-thaw samples. Fluorescence microscopy images were obtained using a Zeiss Axioskop 50 microscope with a 40 × air objective (Plan NeoFluor, NA 0.75; Carl Zeiss) and processed using FIJI ImageJ 2.0.0.

Cells were cultured for 4 days post-thaw to assess cell growth over time. Cells were stained using calcein AM and propidium iodide every 24 h and read using a microplate reader. Amount of cells in the culture was calculated as the ratio of the calcein AM fluorescence level measured at each time point for thawed samples to the mean calcein AM fluorescence level measured at 24 h postpassage of fresh cell controls.

Confocal Raman system

Confocal Raman spectroscopy measurements were conducted using the WITec Confocal Raman Microscope System Alpha 300R with UHTS300 spectrometer and DV401 CCD detector with 600/mm grating. The WITec spectrometer was calibrated with a mercury–argon lamp. The Nd:YAG laser with 532 nm wavelength was used as an excitation source. A 100 × air objective (NA 0.90; Nikon Instruments) was used to focus the 532 nm excitation laser. Laser power at the objective was 10mW, as measured by an optical power meter (THORLABS). Resolution of the microscope was ∼0.3 μm based on Abbe's diffraction formula for lateral resolution.

Raman images were assembled by integrating the spectrum at each pixel based on characteristic wavenumbers of common intracellular and extracellular material (Fig. 1D). Raman signals and the associated wavenumbers selected for these studies are given in Table 1. Amide I and alkyl C = C

Table 1. Wavenumber Assignments for Raman Spectra[31,32]

Substance	*Wavenumber* cm^{-1}	*Assignments*
Protein and lipid (cell)	1660	Amide I and alkyl C = C stretches
Ice	3125	OH stretch
DMSO	673	Symmetric CS stretching

DMSO, dimethyl sulfoxide.

stretches were used to generate a distribution of protein and lipid to delineate the area of frozen single cells or aggregates. Images of ice were generated with background subtraction at both sides of the peak range to separate ice and water signals. The image size for single-cell studies was $15 \times 15\,\mu m$. Each image had 45×45 pixels with an integration of 0.2 s for each pixel. Image size for aggregates varied depending on the actual size of the aggregate. There were two pixels per micrometer for images of aggregates with an integration of 0.2 s for each pixel. Raman signals for this study did not overlap with each other; as a result, multivariate data analysis was not required. IIF was determined by the presence of an OH stretch peak at $3125\,cm^{-1}$. Raman spectra of cell sections with IIF showed the presence of an OH stretch peak, while Raman spectra of cell sections without IIF showed the absence of OH stretch peak (Fig. 1E).

Temperature-controlled stage

Sample temperature for Raman spectroscopy studies was controlled using a four-stage Peltier (Thermonamic Electronics Corp.) and a series 800 temperature controller (Alpha Omega Instruments Corp.). About 1–3 μL of cell suspension was placed on the stage, covered with a piece of mica (TED PELLA), and sealed with Kapton tape (Dupont Wilmington) to prevent evaporation/sublimation. All samples were seeded at −4°C or −8°C with a liquid nitrogen-cooled needle and then cooled to a final temperature of −50°C using the desired cooling rate.

Statistics

Mean plus/minus standard error was reported for all measurements unless otherwise noted. Two-tailed student *t*-tests were performed for two-sample comparisons and one-way ANOVA tests with Tukey HSD were performed for simultaneous three-sample comparisons to obtain *p*-values with significance level set at 0.05. Null hypothesis was defined as no statistical difference between any pair of samples; *p*-value less than 0.05 was used to make the decision of rejecting the null hypothesis and determining the significant difference between samples.

Results

IIF of cryopreserved hiPSCs

IIF can be influenced by many freezing parameters, including cell type, cell–cell interaction, cooling rate, seeding temperature, and solution composition.[4] To investigate the effects of cooling rates and seeding temperatures on the IIF of cryopreserved hiPSCs, single cells and aggregates in 10% DMSO solution were frozen at a constant cooling rate of 1, 3, or 10°C/min with seeding temperature of −4°C or −8°C.

Typical Raman images rendered on the signal associated with ice and amide I are shown for both single cells and aggregates cryopreserved at three different cooling rates grouped by seeding temperatures (Fig. 2A, B, D, and E). To characterize the proportion of IIF, the ratio of cross-sectional area of IIF to the cross-sectional area of single cells or aggregates area ratio of intracellular ice to cell (AIC) was calculated. The effect of cooling rates on AIC was examined for a given seeding temperature. For single cells, there is no statistical difference of AIC between cells cryopreserved at 1 and 3°C/min; however, cells cryopreserved at 10°C/min showed statistically greater AIC for both seeding temperatures (Fig. 2C). Similar conclusions on the effect of cooling rates on AIC can be drawn for aggregates (Fig. 2F).

The effects of seeding temperature on AIC were also investigated. There was no statistical difference in AIC between single cells seeded at −4°C and −8°C for all three cooling rates (see Supplementary Fig. S1; Supplementary Data available online at www.libertpub.com/tec). For aggregates, greater AIC was observed at a seeding temperature of −8°C than −4°C for a cooling rate of 1 and 3°C/min. Aggregates cryopreserved at 10°C/min showed no difference in AIC between the two seeding temperatures (Fig. 2G).

DMSO distribution of cryopreserved hiPSCs

Single cells and aggregates frozen without a significant amount of IIF were used to study whether the distribution of DMSO varied in aggregates.[34] Raman images of DMSO in cells frozen at 1°C/min and seeded at −4°C are shown as examples (Fig. 3A and B). For single cells, a diagonal line was drawn across the image and the normalized DMSO concentration (DMSO peak intensity at each pixel to the maximum DMSO peak intensity of the line) was calculated (Fig. 3A). Standard deviation (SD) of normalized DMSO concentration was calculated to represent the variation of DMSO concentration across the cell. It was noteworthy that 1 μm from the cell membrane inward to the cell was not considered for the calculation because of partitioning of DMSO by the cell membrane (calculation within gray shading). For aggregates, two diagonal lines were drawn across the image and the DMSO concentration along those lines as well as its variation was quantified. It was found that SD was significantly greater in aggregates than single cells frozen at 1 or 3°C/min (Fig. 3C).

Post-thaw membrane integrity and attachment of cryopreserved hiPSCs

Post-thaw recovery and attachment rates were examined for both hiPSCs as single cells and aggregates cryopreserved using CRF with the same set of cooling rates, 1, 3, and 10°C/min, and seeding temperatures, −4°C and −8°C. Post-thaw recovery was measured in terms of membrane integrity. Post-thaw attachment was normalized to the postpassage attachment of fresh nonfrozen aggregates, so a post-thaw attachment rate close to one indicates attachment ability of cryopreserved cells comparable with what was observed for fresh cells. Of all freezing conditions tested, the combined cooling rate of 1°C/min and seeding temperature of −4°C had the highest mean post-thaw recovery at 97.93% and highest mean post-thaw attachment rate at 0.9851.

The effect of different cooling rates was examined for each seeding temperature. For single cells, membrane integrity for both 1 and 3°C/min was significantly higher than 10°C/min regardless of the seeding temperature (Fig. 4A). All the single-cell conditions tested had few to no cells attached to the culture substrate post-thaw (Fig. 4C), consistent with previous studies.[36–38] For aggregates, little difference in membrane integrity was observed for the range of cooling rates studied (Fig. 4B). However, aggregates cryopreserved at 1°C/min attached to the surface post-thaw at greater rates than either 3 or 10°C/min for a seeding temperature of −4°C (Fig. 4D). The effect of different

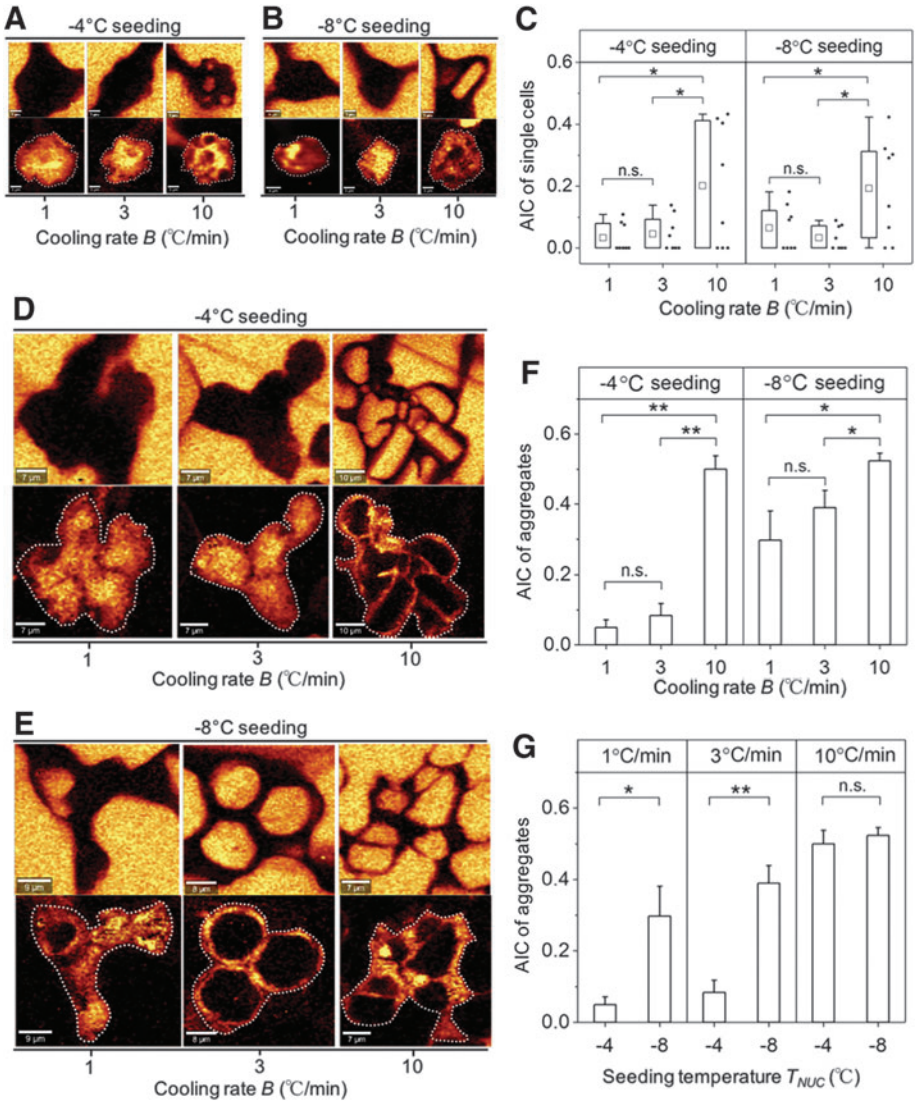

FIG. 2. **(A)** Raman images of ice and amide I of single cells at seeding temperature of −4°C. **(B)** Raman images of ice and amide I of single cells at seeding temperature of −8°C. **(C)** AIC of single cells grouped by seeding temperature ($n=8$, $^*p<0.05$). Ends of the whiskers represent the minimum and maximum of the data. The *bottom* and *top* of the box are the first and third quartiles and the *square* inside the box is the average. **(D)** Raman images of ice and amide I of aggregates at seeding temperature of −4°C. **(E)** Raman images of ice and amide I of aggregates at seeding temperature of −8°C. **(F)** AIC of aggregates grouped by seeding temperature (SE, $n=5$, $^*p<0.05$, $^{**}p<0.01$). **(G)** AIC of aggregates grouped by cooling rates (SE, $n=5$, $^*p<0.05$, $^{**}p<0.01$). AIC, area ratio of intracellular ice to cell.

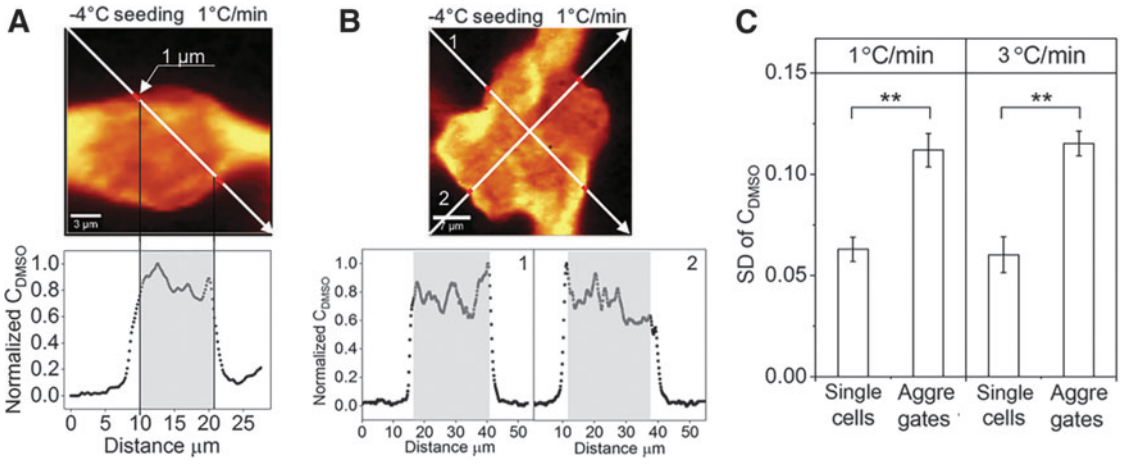

FIG. 3. **(A)** Raman image of DMSO in single hiPSCs cryopreserved at 1°C/min with seeding temperature of −4°C (scale bar: 3 μm). The *white arrow* goes through different regions of the image and represents the location where peak intensity of DMSO is obtained. Normalized DMSO concentration (peak intensity of DMSO at each data point along the *arrow* divided by maximum peak intensity of DMSO) is plotted as a function of horizontal distance of the *arrow* from its start point. *Gray* shading indicates the region used for calculation of SD of normalized DMSO concentration. **(B)** Raman image of DMSO of aggregates cryopreserved at 1°C/min with seeding temperature of −4°C (scale bar: 7 μm). Normalized DMSO is plotted as a function of horizontal distance of the *arrow* from its start point for both *arrows*. **(C)** SD of normalized DMSO concentration for single cells and aggregates cryopreserved at 1°C and 3°C with seeding temperature of −4°C (SE, $n=8$ for single cells, $n=5$ for aggregates, $^{**}p<0.01$). SD, standard deviation.

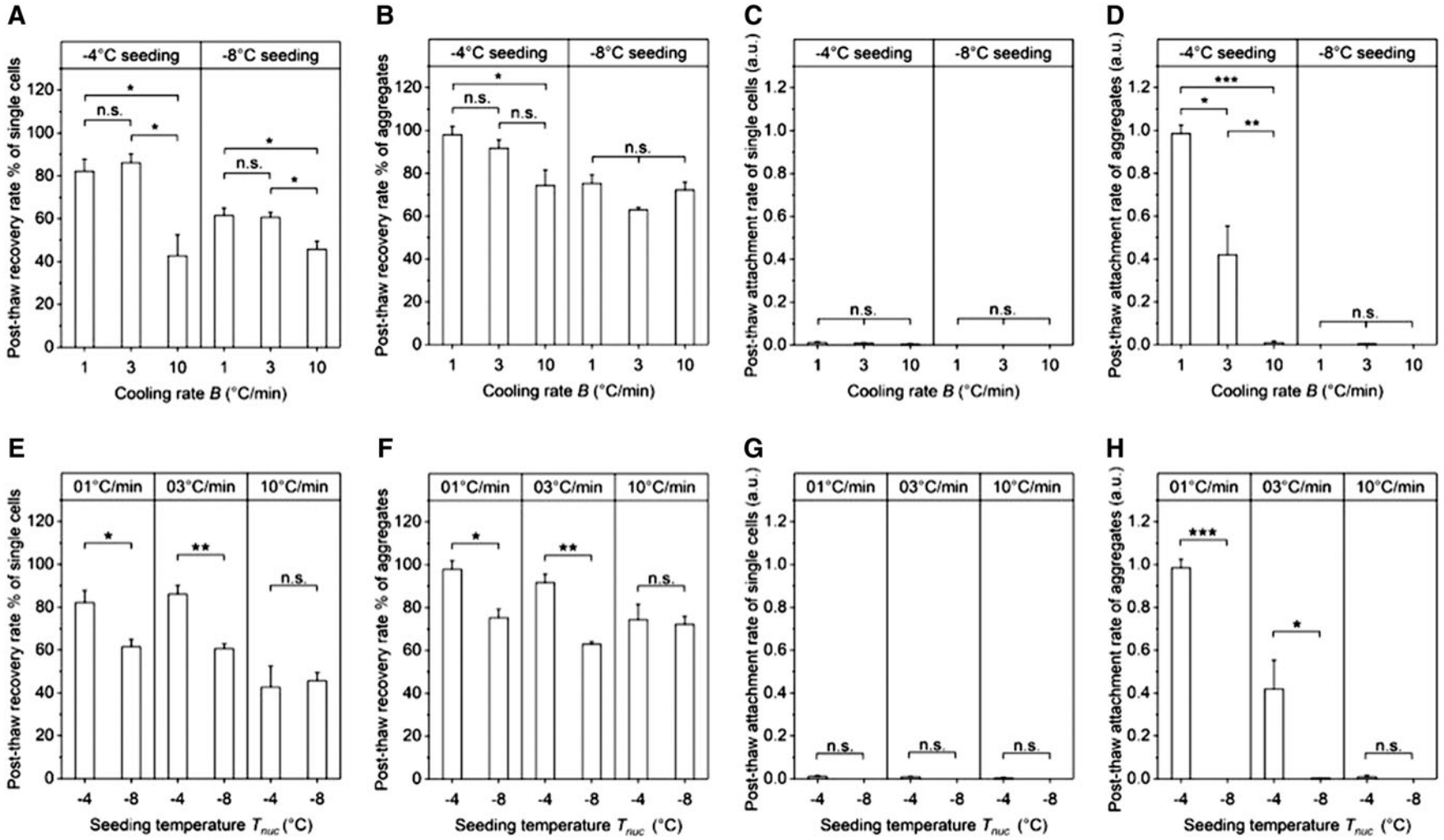

FIG. 4. **(A)** Post-thaw recovery rate of single cells against cooling rate grouped by seeding temperature. **(B)** Post-thaw recovery rate of aggregates against cooling rate grouped by seeding temperature. **(C)** Post-thaw attachment rate of single cells against cooling rate grouped by seeding temperature. **(D)** Post-thaw attachment rate of aggregates against cooling rate grouped by seeding temperature. **(E)** Post-thaw recovery rate of single cells against seeding temperature grouped by cooling rate. **(F)** Post-thaw recovery rate of aggregates against seeding temperature grouped by cooling rate. **(G)** Post-thaw attachment rate of single cells against seeding temperature grouped by cooling rate. **(H)** Post-thaw attachment rate of aggregates against seeding temperature grouped by cooling rate. (SE, $n = 3$, n.s.: $p \geq 0.05$, $^{*}p < 0.05$, $^{**}p < 0.01$, $^{***}p < 0.001$).

seeding temperatures was examined for each cooling rate. For cells frozen at 1 and 3°C/min, membrane integrity (of both single cells and aggregates, Fig. 4E, F) and cell attachment (of aggregates, Fig. 4H) for seeding temperature of −4°C were significantly higher than −8°C; for those frozen at 10°C/min, little difference in membrane integrity or cell attachment was observed for the seeding temperatures studied (Fig. 4E–H).

Apoptosis and proliferation in post-thaw culture of cryopreserved hiPSC aggregates

In many different cell types, post-thaw apoptosis can result in significant cell losses.[39,40] As a result, we investigated both post-thaw apoptosis and proliferation. The proportions of apoptotic and necrotic subpopulations were measured (Fig. 5A) for all cryopreserved cell aggregate samples immediately post-thaw, as well as a fresh cell aggregate control immediately after dissociation from culture, by detecting caspase activation and membrane integrity. All samples, including the postpassage control, had large proportions of cells expressing apoptosis markers (64% to 78% of total cell population, Fig. 5B). The ratio of early to late apoptotic subpopulations was also calculated. Freezing at higher cooling rates resulted in two- to threefold less predominantly early apoptosis and more late apoptosis (Fig. 5B). No obvious difference in apoptotic subpopulations was observed between the different seeding temperatures at each cooling rate.

Post-thaw apoptosis was further monitored through chromatin condensation in attached colonies for up to 24 h post-thaw. Condensed chromatin was not visible at 4 h

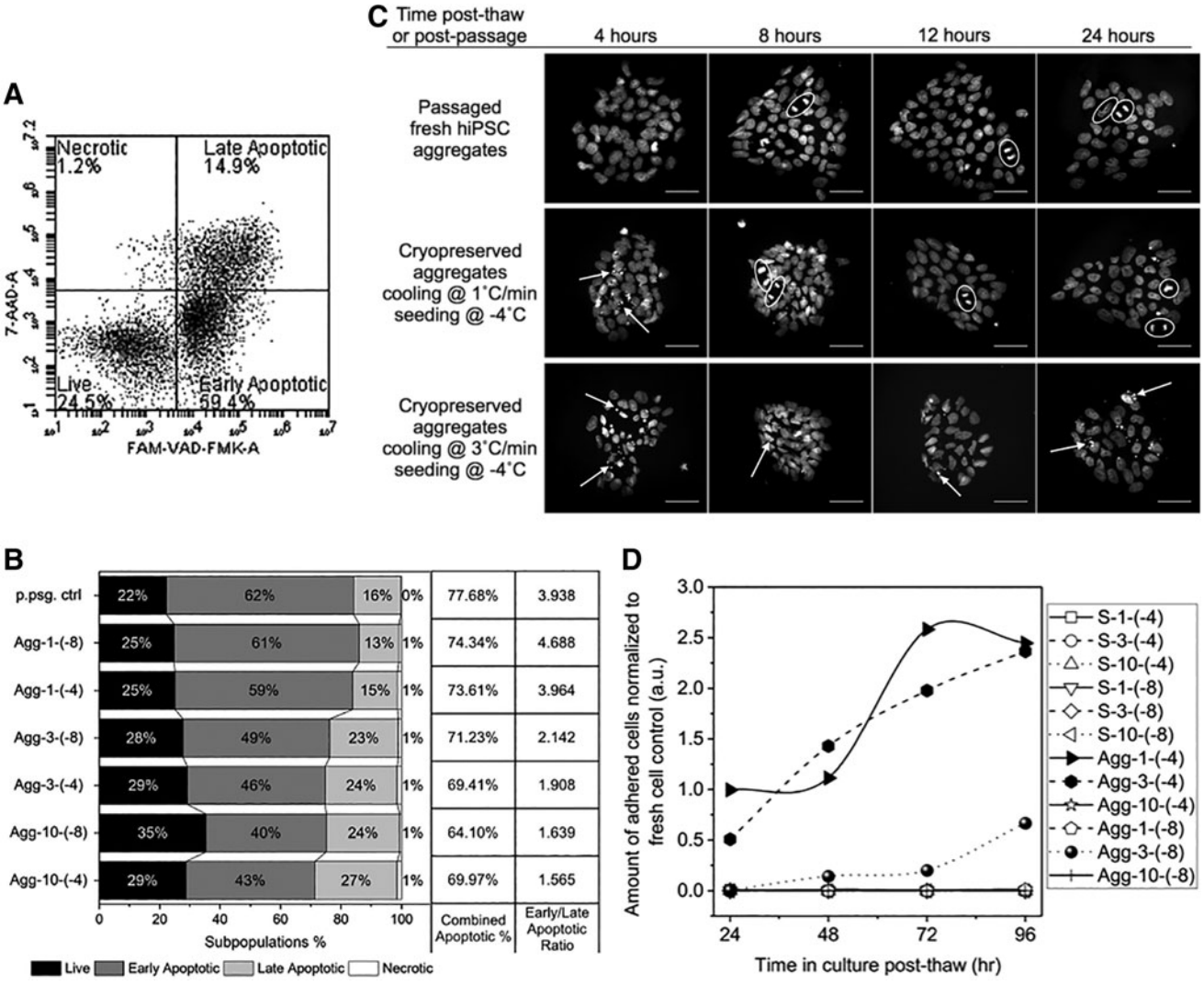

FIG. 5. **(A)** An example of flow cytometry density plot of FAM-VAD-FMK against 7-AAD, with four quadrants defining live, early apoptotic, late apoptotic, and necrotic cell subpopulations, respectively. **(B)** *Left*: 100% stacked *column* graph of cell subpopulation proportions against fresh postpassage control or freezing condition in abbreviated forms: aggregates-cooling rate (°C/min)-seeding temperature (°C). *Right*: combined apoptotic population proportion and ratio of early to late apoptotic population proportions calculated from the subpopulation proportions on the *left*. **(C)** Attached colonies in culture 4, 8, 12, and 24 h postpassage or post-thaw, stained with Hoechst 33342. *White arrows* point at condensed chromatin. *White circles* highlight formed, aligned, or separated sister chromatids (scale bar: 50 μm). **(D)** Modified Bezier curves of cell growth up to 4 days post-thaw. Sample conditions are shown in abbreviated forms: single cells (or aggregates)-cooling rate (°C/min)-seeding temperature (°C).

postpassage, but was visible until 8 h post-thaw for aggregates frozen at 1°C/min and seeded at −4°C and up to 24 h post-thaw for aggregates frozen at 3°C/min and seeded at −4°C (Fig. 5C). In addition, sister chromatids were also clearly visible starting at 8 h postpassage; 8 h post-thaw for aggregates frozen at 1°C/min and seeded at −4°C, but not observed for aggregates frozen at 3°C/min and seeded at −4°C. As shown by growth curves in Figure 5D, the aggregates frozen at 3°C/min and seeded at −4°C proliferated greatly between 24 and 48 h post-thaw, surpassing the culture of aggregates frozen at 1°C/min and seeded at −4°C; the culture of aggregates frozen at 3°C/min and seeded at −8°C proliferated and became detectable starting at 48 h post-thaw; all the rest of the sample conditions, single cells and aggregates, did not show detectable amounts of attached cells throughout the 4-day period.

Discussion

IIF mechanism and ice crystal propagation

AIC values of single cells and aggregates cryopreserved at 10°C/min were significantly greater than those at 1 and 3°C/min, consistent with earlier studies that fast cooling rates resulted in greater IIF[41] and a greater value of AIC led to lower cell survival.[34] Two different types of ice crystals were observed in this study: (1) small ice crystals mixed with cytoplasm and (2) large pure ice crystals (Fig. 6A). Type-1 ice crystals were intracellular, as observed in a previous study[34]; type-2 ice crystals could be either intracellular or intercellular, where future study is needed to determine its location relative to the cell membrane. However, because the size of some type-2 ice crystals was clearly greater than that of an individual cell, they were most likely intercellular. Only the high cooling rate (10°C/min) resulted in type-2 ice crystals in cryopreserved single cells. The relative insensitivity of hiPSC single cells to supercooling is similar to that observed with peripheral lymphocytes,[42] but differs from hepatocytes,[43] erythrocytes,[44] and hiPSC aggregates. In contrast, a high cooling rate (10°C/min) and low seeding temperature (−8°C) resulted in type-2 ice crystals in aggregates. This suggests that aggregates are more sensitive to seeding temperature than single cells. As the seeding temperature decreased from −4°C to −8°C, the cooling rate threshold for IIF in aggregates also decreased from 10°C/min to 1°C/min, which is consistent with an early study, where the higher the degree of supercooling, the lower the cooling rate at which IIF is observed.[44]

A lower seeding temperature results in a greater difference in chemical potential across the cell membrane.[45] It has been hypothesized that a new equilibrium can be reached by dehydration of cells or solidification of water inside the cell. Several effects could influence the probability of IIF at lower seeding temperatures, including water permeability of the cell membrane. Compared with single cells, aggregates

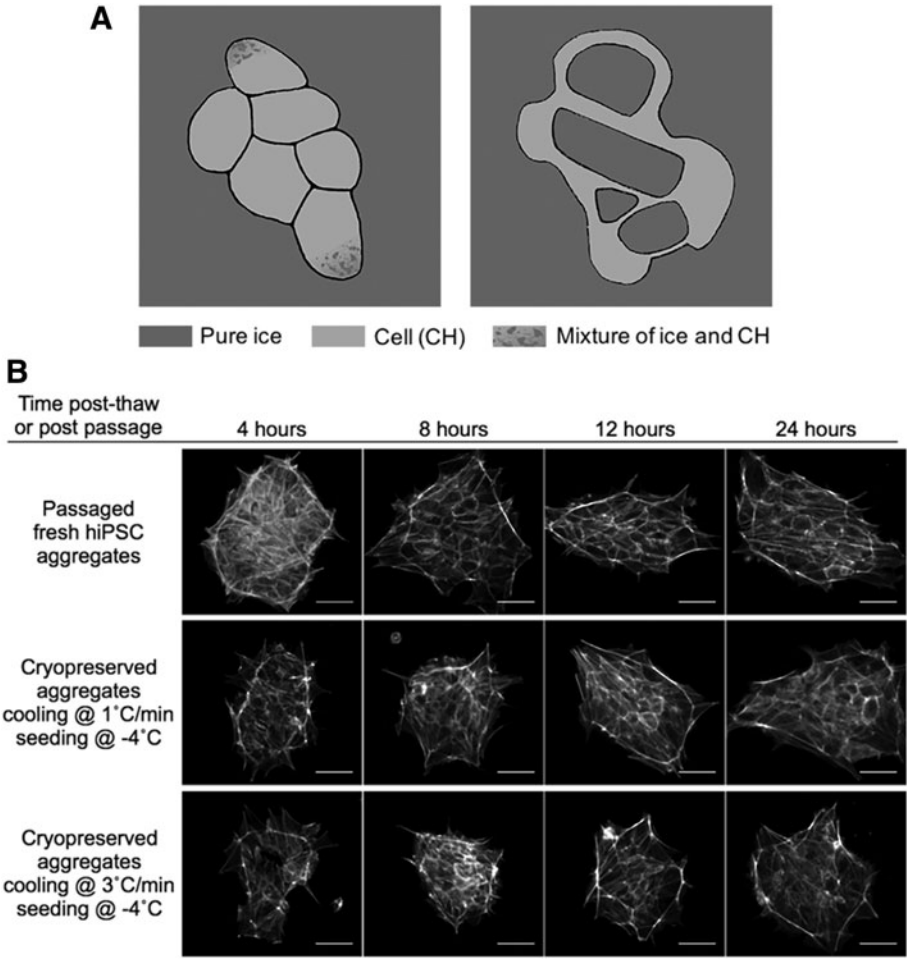

FIG. 6. **(A)** Sketches of frozen cell aggregates showing two types of ice crystals. Type 1 crystals are small crystals mixed with cytoplasm (figure on left) and Type 2 crystals are large chunks of ice (figure on right). **(B)** Attached colonies in culture 4, 8, 12, and 24 h postpassage or post-thaw, stained for f-actin. The honeycomb-like pattern became clearly visible around 8 h post-passage and around 12 h post-thaw for aggregates cryopreserved at 1°C/min with seeding at −4°C and for those cryopreserved at 3°C/min with seeding at −4°C. All other freezing conditions tested were not assessed here due to failed post-thaw cell attachment (scale bar: 50 μm).

have a more complex cytoskeletal structure (Fig. 6B), which can interact with the plasma membrane, compacting the aggregates,[46] therefore decreasing membrane water permeability.[47] The higher sensitivity to supercooling of aggregates than single cells may be a result of this decreased membrane water permeability.

Propagation of ice crystals from cell to cell has been observed in non-hiPSC aggregates.[5–8] In this study, small ice crystals mixed with cytoplasm were confined within the cell where ice was initially formed, and there was no evidence that these small ice crystals propagated from one cell to the next.

DMSO distribution between single cells and aggregates

Variation of DMSO concentration across aggregates was significantly greater than that across single cells frozen at cooling rates 1 and 3°C/min with seeding temperature of −4°C. These differences could result from greater disturbance to transport by more complex membrane–cytoskeletal structure[46] of multicellular systems. Previous studies have measured DMSO transport in tissues using MRI[48] and demonstrated variations in the concentration with time and location, but no previous studies have had the spatial resolution to look at the distribution of cryoprotectants in a multicellular system on a cell-by-cell basis. Raman spectroscopy served as an ideal tool to investigate the distribution of cryoprotectant cell by cell for both single cells and multicellular aggregates in this study.

Membrane integrity, cell attachment, and IIF

For single cells, similar to what was reported in literature,[14–17] slow cooling rates (1 and 3°C/min) allowed significantly better preservation of membrane integrity than a higher cooling rate (10°C/min) regardless of the seeding temperature. This outcome was consistent with the observation that AIC increased with increasing cooling rate.

For aggregates, however, slow cooling rates (1 and 3°C/min) combined with high seeding temperature (−4°C) had little effect on membrane integrity, but resulted in significantly better cell attachment than a higher cooling rate (10°C/min) or low seeding temperature (−8°C). The clear advantage of seeding temperature of −4°C compared with −8°C suggests that the range of seeding temperatures of −7°C to −12°C being used in literature[13] is suboptimal and that seeding temperature should be considered as a critical parameter when designing a cryopreservation protocol for hiPSCs. Cell attachment of aggregates correlated with AIC. The two freezing conditions that successfully attached post-thaw had little intracellular ice, while those freezing conditions that formed large pure ice crystals failed to attach post-thaw. Similar to the results observed with human mesenchymal stem cells (hMSCs),[49] membrane integrity of hiPSC aggregates did not always correlate with cell attachment. All conditions tested using aggregates had reasonable levels of post-thaw membrane integrity, but only two of these conditions had detectable cell attachment post-thaw (Fig. 4). The specific mechanism for impaired attachment observed in this study is not clear. Previous studies have found that freezing can result in damage to cytoskeleton[50] or exposure to DMSO can result in damage to DNA and protein[51,52] that does not alter membrane integrity. This suggested that the two metrics, post-thaw recovery rate and post-thaw attachment rate, could be decoupled. The conventional approach of optimizing hiPSC cryopreservation based on only post-thaw membrane integrity may be insufficient. Functional metrics such as post-thaw attachment should be incorporated into screening of cryoprotectants and tuning of freezing protocols.

Post-thaw behavior of hiPSC aggregates

Post-thaw apoptosis can influence the persistence of cells with time post-thaw. Significant cell losses can be experienced with time post-thaw, resulting from apoptosis.[40] High levels of post-thaw apoptosis were observed in this investigation and apoptosis dominated necrosis. This result is similar to that observed in renal cells and hESCs.[40,53] However, unlike hematopoietic stem cells[54,55] and lymphocytes,[56] no association between caspase activation (early apoptosis) and post-thaw function (cell attachment) was found in cryopreserved hiPSC aggregates. Different freezing conditions resulted in similar levels of caspase activation. A similar level of caspase activation was also observed in passaged fresh hiPSC aggregates, suggesting that the high caspase activation was primarily induced by cell dissociation rather than cryopreservation.[36] The presence of condensed chromatin (late apoptosis) and absence of mitotic chromosomes (proliferation) up to 24 h post-thaw correlated with low cell attachment measured at 24 h post-thaw.

F-actin cytoskeleton has been evaluated by previous studies in ROCKi-conditioned adherent single cells.[57] In this study, f-actin cytoskeletal organization was monitored in attached colonies of ROCKi-free culture (Fig. 6B). The colonies underwent remodeling and reestablishing of f-actin organization, both post-thaw, in the cryopreserved samples and postpassage in the fresh sample where f-actin fibers progressed to localize near cell–cell interfaces and the edge of the colony, forming a honeycomb-like pattern. Impaired f-actin organization was seen in cryopreserved cells up to 8 h post-thaw compared with fresh cells, which could be explained by actin depolymerization due to osmotic stress during the freeze–thaw process.[50] Dense f-actin at the edge of the colony was identified in a recent study as a contractile actin fence that reinforces colony structure and pluripotency,[46] supporting the observation that the f-actin organization plays an important role in post-thaw survival and growth of these multicellular aggregates.

Another recent study found that survival of cryopreserved aggregates depended on the size of aggregates, preferring those around 109 μm in diameter to larger sizes.[58] Combined with our findings, it is clear that hiPSCs as a multicellular system respond to freezing in a very complex manner, and successful establishment of post-thaw culture depends on various critical factors. Further studies will need to not only continue exploring additional factors to optimize the freezing protocol for hiPSCs but also investigate biological pathways connecting the factors and the observed cryopreservation outcomes to provide targets for future development of cryoprotectants.

Acknowledgments

This work was funded by R01EB023880. Parts of this work were carried out in the Characterization Facility, University of

Minnesota, which receives partial support from NSF through the MRSEC program. The authors thank their colleagues at Ogle laboratory in the Department of Biomedical Engineering for providing the flow cytometry system.

Disclosure Statement

No competing financial interests exist.

References

1. Yu, J., Vodyanik, M.A., Smuga-Otto, K., *et al*. Induced pluripotent stem cell lines derived from human somatic cells. Science **318,** 1917, 2007.
2. Yu, J., Hu, K., Smuga-Otto, K., *et al*. Human induced pluripotent stem cells free of vector and transgene sequences. Science **324,** 797, 2009.
3. Bastami, F., Nazeman, P., Moslemi, H., Rezai Rad, M., Sharifi, K., and Khojasteh, A. Induced pluripotent stem cells as a new getaway for bone tissue engineering: a systematic review. Cell Prolif **50,** e12321, 2017.
4. Mihara, Y., Matsuura, K., Sakamoto, Y., Okano, T., Kokudo, N., and Shimizu, T. Production of pancreatic progenitor cells from human induced pluripotent stem cells using a three-dimensional suspension bioreactor system. J Tissue Eng Regen Med **11,** 3193, 2017.
5. Gao, L., Kupfer, M.E., Jung, J.P., *et al*. Myocardial tissue engineering with cells derived from human-induced pluripotent stem cells and a native-like, high-resolution, 3-dimensionally printed scaffold. Circ Res **120,** 1318, 2017.
6. Madonna, R. Human-induced pluripotent stem cells: in quest of clinical applications. Mol Biotechnol **52,** 193, 2012.
7. Singh, V.K., Kalsan, M., Kumar, N., Saini, A., and Chandra, R. Induced pluripotent stem cells: applications in regenerative medicine, disease modeling, and drug discovery. Front Cell Dev Biol **3,** 2, 2015.
8. Matsa, E., Ahrens, J.H., and Wu, J.C. Human induced pluripotent stem cells as a platform for personalized and precision cardiovascular medicine. Physiol Rev **96,** 1093, 2016.
9. Chun, Y.S., Byun, K., and Lee, B. Induced pluripotent stem cells and personalized medicine: current progress and future perspectives. Anat Cell Biol **44,** 245, 2011.
10. Crook, J.M., Tomaskovic-Crook, E., and Ludwig, T.E. Cryobanking pluripotent stem cells. Methods Mol Biol **1590,** 151, 2017.
11. Hunt, C.J. Cryopreservation of human stem cells for clinical application: a review. Transfus Med Hemother **38,** 107, 2011.
12. Martin-Ibanez, R., Hovatta, O., and Canals, J. M. cryopreservation of human pluripotent stem cells: are we going in the right direction? In: Katkov, I., ed. Current Frontiers in Cryobiology, Rijeka, Croatia: InTech, 2012, pp. 139–166.
13. Li, Y., and Ma, T. Bioprocessing of cryopreservation for large-scale banking of human pluripotent stem cells. BioRes Open Access **1,** 205, 2012.
14. Valbuena, D., Sanchez-Luengo, S., Galan, A., *et al*. Efficient method for slow cryopreservation of human embryonic stem cells in xeno-free conditions. Reprod Biomed Online **17,** 127, 2008.
15. Lee, J.Y., Lee, J.E., Kim, D.K., Yoon, T.K., Chung, H.M., and Lee, D.R. High concentration of synthetic serum, stepwise equilibration and slow cooling as an efficient technique for large-scale cryopreservation of human embryonic stem cells. Fertil Steril **93,** 976, 2010.
16. Yang, P.F., Hua, T.C., Wu, J., Chang, Z.H., Tsung, H.C., and Cao, Y.L. Cryopreservation of human embryonic stem cells: a protocol by programmed cooling. Cryo Letters **27,** 361, 2006.
17. Ware, C.B., Nelson, A.M., and Blau, C.A. Controlled-rate freezing of human ES cells. Biotechniques **38,** 879, 2005.
18. John, G., and Baust, J.M.B. Advances in Biopreservation. Boca Raton, FL: CRC Press, 2006.
19. Li, X., Meng, G., Krawetz, R., Liu, S., and Rancourt, D.E. The ROCK inhibitor Y-27632 enhances the survival rate of human embryonic stem cells following cryopreservation. Stem Cells Dev **17,** 1079, 2008.
20. Claassen, D.A., Desler, M.M., and Rizzino, A. ROCK inhibition enhances the recovery and growth of cryopreserved human embryonic stem cells and human induced pluripotent stem cells. Mol Reprod Dev **76,** 722, 2009.
21. Mollamohammadi, S., Taei, A., Pakzad, M., *et al*. A simple and efficient cryopreservation method for feeder-free dissociated human induced pluripotent stem cells and human embryonic stem cells. Hum Reprod **24,** 2468, 2009.
22. Chen, G., Hou, Z., Gulbranson, D.R., and Thomson, J.A. Actin-myosin contractility is responsible for the reduced viability of dissociated human embryonic stem cells. Cell Stem Cell **7,** 240, 2010.
23. Walker, A., Su, H., Conti, M.A., Harb, N., Adelstein, R.S., and Sato, N. Non-muscle myosin II regulates survival threshold of pluripotent stem cells. Nat Commun **1,** 71, 2010.
24. Vicente-Manzanares, M., Ma, X., Adelstein, R.S., and Horwitz, A.R. Non-muscle myosin II takes centre stage in cell adhesion and migration. Nat Rev Mol Cell Biol **10,** 778, 2009.
25. Li, D., Zhou, J., Wang, L., *et al*. Integrated biochemical and mechanical signals regulate multifaceted human embryonic stem cell functions. J Cell Biol **191,** 631, 2010.
26. Fuller, B.J. Life in the Frozen State. Boca Raton, FL: CRC Press, 2004.
27. Acker, J.P., Elliott, J.A., and McGann, L.E. Intercellular ice propagation: experimental evidence for ice growth through membrane pores. Biophys J **81,** 1389, 2001.
28. Irimia, D., and Karlsson, J.O. Kinetics and mechanism of intercellular ice propagation in a micropatterned tissue construct. Biophys J **82,** 1858, 2002.
29. Berger, W.K., and Uhrik, B. Freeze-induced shrinkage of individual cells and cell-to-cell propagation of intracellular ice in cell chains from salivary glands. Experientia **52,** 843, 1996.
30. Pollock, K., Yu, G., Moller-Trane, R., *et al*. Combinations of osmolytes, including monosaccharides, disaccharides, and sugar alcohols act in concert during cryopreservation to improve mesenchymal stromal cell survival. Tissue Eng Part C Methods **22,** 999, 2016.
31. Dong, J., Malsam, J., Bischof, J.C., Hubel, A., and Aksan, A. Spatial distribution of the state of water in frozen mammalian cells. Biophys J **99,** 2453, 2010.
32. Kreiner-Moller, A., Stracke, F., and Zimmermann, H. Hydrohalite spatial distribution in frozen cell cultures measured using confocal Raman microscopy. Cryobiology **69,** 41, 2014.
33. Okotrub, K.A., and Surovtsev, N.V. Raman scattering evidence of hydrohalite formation on frozen yeast cells. Cryobiology **66,** 47, 2013.
34. Yu, G., Yap, Y.R., Pollock, K., and Hubel, A. Characterizing intracellular ice formation of lymphoblasts using low-temperature Raman spectroscopy. Biophys J **112,** 2653, 2017.
35. Dong, J., Hubel, A., Bischof, J.C., and Aksan, A. Freezing-induced phase separation and spatial microheterogeneity in protein solutions. J Phys Chem B **113,** 10081, 2009.

36. Ohgushi, M., Matsumura, M., Eiraku, M., *et al*. Molecular pathway and cell state responsible for dissociation-induced apoptosis in human pluripotent stem cells. Cell Stem Cell **7,** 225, 2010.
37. Katkov, I.I., Kan, N.G., Cimadamore, F., Nelson, B., Snyder, E.Y., and Terskikh, A.V. DMSO-free programmed cryopreservation of fully dissociated and adherent human induced pluripotent stem cells. Stem Cells Int **2011,** 981606, 2011.
38. Watanabe, K., Ueno, M., Kamiya, D., *et al*. A ROCK inhibitor permits survival of dissociated human embryonic stem cells. Nat Biotechnol **25,** 681, 2007.
39. Sasnoor, L.M., Kale, V.P., and Limaye, L.S. Prevention of apoptosis as a possible mechanism behind improved cryoprotection of hematopoietic cells by catalase and trehalose. Transplantation **80,** 1251, 2005.
40. Baust, J.M., Van, B., and Baust, J.G. Cell viability improves following inhibition of cryopreservation-induced apoptosis. In Vitro Cell Dev Biol Anim **36,** 262, 2000.
41. Mazur, P. Freezing of living cells: mechanisms and implications. Am J Physiol **247,** C125, 1984.
42. Foreman, J., and Pegg, D.E. Cell preservation in a programmed cooling machine: the effect of variations in supercooling. Cryobiology **16,** 315, 1979.
43. Harris, C.L., Toner, M., Hubel, A., Cravalho, E.G., Yarmush, M.L., and Tompkins, R.G. Cryopreservation of isolated hepatocytes: intracellular ice formation under various chemical and physical conditions. Cryobiology **28,** 436, 1991.
44. Diller, K.R. Intracellular freezing: effect of extracellular supercooling. Cryobiology **12,** 480, 1975.
45. Toner, M. Nucleation of ice crystals inside biological cells. In: Steponkus, P., ed. Advances in Low Temperature Biology. London: JAI Press, 1993, p. 1.
46. Narva, E., Stubb, A., Guzman, C., *et al.* A strong contractile actin fence and large adhesions direct human pluripotent colony morphology and adhesion. Stem Cell Rep **9,** 67, 2017.
47. Noiles, E.E., Thompson, K.A., and Storey, B.T. Water permeability, Lp, of the mouse sperm plasma membrane and its activation energy are strongly dependent on interaction of the plasma membrane with the sperm cytoskeleton. Cryobiology **35,** 79, 1997.
48. Bidault, N.P., Hammer, B.E., and Hubel, A. Water content in an engineered dermal replacement during permeation of Me2SO solutions using rapid MR imaging. Biotechnol Prog **17,** 530, 2001.
49. Pollock, K., Sumstad, D., Kadidlo, D., McKenna, D.H., and Hubel, A. Clinical mesenchymal stromal cell products undergo functional changes in response to freezing. Cytotherapy **17,** 38, 2015.
50. Ragoonanan, V., Hubel, A., and Aksan, A. Response of the cell membrane-cytoskeleton complex to osmotic and freeze/thaw stresses. Cryobiology **61,** 335, 2010.
51. Fahy, G.M., Lilley, T.H., Linsdell, H., Douglas, M.S., and Meryman, H.T. Cryoprotectant toxicity and cryoprotectant toxicity reduction: in search of molecular mechanisms. Cryobiology **27,** 247, 1990.
52. Gao, D., and Critser, J.K. Mechanisms of cryoinjury in living cells. ILAR J **41,** 187, 2000.
53. Heng, B.C., Ye, C.P., Liu, H., *et al*. Loss of viability during freeze-thaw of intact and adherent human embryonic stem cells with conventional slow-cooling protocols is predominantly due to apoptosis rather than cellular necrosis. J Biomed Sci **13,** 433, 2006.
54. de Boer, F., Drager, A.M., Pinedo, H.M., *et al*. Early apoptosis largely accounts for functional impairment of CD34+ cells in frozen-thawed stem cell grafts. J Hematother Stem Cell Res **11,** 951, 2002.
55. Stroh, C., Cassens, U., Samraj, A., Sibrowski, W., Schulze-Osthoff, K., and Los, M. The role of caspases in cryoinjury: caspase inhibition strongly improves the recovery of cryopreserved hematopoietic and other cells. FASEB J **16,** 1651, 2002.
56. Fowke, K.R., Behnke, J., Hanson, C., Shea, K., and Cosentino, L.M. Apoptosis: a method for evaluating the cryopreservation of whole blood and peripheral blood mononuclear cells. J Immunol Methods **244,** 139, 2000.
57. Boraas, L.C., Guidry, J.B., Pineda, E.T., and Ahsan, T. Cytoskeletal expression and remodeling in pluripotent stem cells. PLoS One **11,** e0145084, 2016.
58. Sart, S., Ma, T., and Li, Y. Cryopreservation of pluripotent stem cell aggregates in defined protein-free formulation. Biotechnol Prog **29,** 143, 2013.

Address correspondence to:
Allison Hubel, PhD
Department of Mechanical Engineering
University of Minnesota
111 Church St. SE
Minneapolis, MN 55455

E-mail: hubel001@umn.edu

Received: December 23, 2017
Accepted: February 22, 2018
Online Publication Date: March 28, 2018